Gap structure probed by field-angle resolved thermal oscillations in $A_y Fe_2Se_2$ superconductors

Tanmoy Das[1], Anton B. Vorontsov[2], Ilya Vekhter[3], and Matthias J. Graf[1]
[1] *Theoretical Division, Los Alamos National Laboratory, Los Alamos, New Mexico 87545, USA*
[2] *Department of Physics, Montana State University, Bozeman, Montana 59717, USA*
[3] *Department of Physics and Astronomy, Louisiana State University, Baton Rouge, Louisiana 70803, USA*
(Dated: March 13, 2012)

We present a numerical study of the angle-resolved oscillations of the thermal conductivity and specific heat under rotated magnetic field in the $A_yFe_2Se_2$ [A=K,Cs,(Tl,K)] superconductors, using realistic two-band Fermi surface parameterization. We find that even for isotropic pairing over an anisotropic Fermi surface, the thermodynamic quantities exhibit substantial oscillatory behavior in the superconducting state beyond that due to the anisotropy of the upper critical field. Furthermore, in multiband systems the competition of anisotropies between two Fermi surfaces can cause a double sign-reversal of the oscillations as a function of temperature, irrespective of gap anisotropy. Our findings put severe constraints on simple interpretations of field-angle resolved measurements used to identify the angular structure of the superconducting gap.

PACS numbers: 74.20.Rp,74.70.Xa,74.25.Uv,74.25.N-

Introduction– The identification of the symmetry of the superconducting (SC) order parameter (OP) is an important step toward unraveling the origin of the pairing mechanism in any novel superconductor. For iron-pnictides, the presence of hole and electron pockets at the Γ and M points led to the proposal of $s^{\pm}$-wave pairing [1–4] due to interband nesting. However, the recent discovery of the layered $A_yFe_2Se_2$, with A=K,Cs,(Tl,K), high-temperature superconductors has challenged the consensus for the pairing symmetry and mechanism of superconductivity in this class of materials [5]. The iron-selenide family has a crystal structure similar to the $BaFe_2As_2$ iron-pnictides, but with hole pockets eliminated completely from the Fermi surface, yet the superconducting transition temperature T_c is comparable to that of iron-pnictides. Various theoretical proposals have been put forward which support either the survival of s-wave pairing [6, 7], the emergence of nodal d-wave OP [8], or nodeless d-wave OP [9–11]. Indirect experimental evidence suggests isotropic pairing symmetry [12–14]. Therefore, direct imaging of the structure of the gap function and the location of the nodes, if they exist, is required. An effective and accurate technique for measuring the angular structure of the bulk OP relies on probing thermodynamic properties in a rotating in-plane magnetic field. For cuprates, pnictides, and heavy-fermion superconductors, this technique has been used successfully to identify the pairing symmetry by directly mapping the field-angle dependence of the thermal conductivity and specific heat one-to-one onto the angular structure of the OP and its pairing symmetry [15–17].

In this Letter, we demonstrate that detailed knowledge of the Fermi surface (FS) topology and parameters are necessary for mapping oscillations onto nodes of the OP. This is especially important for materials, where the FS anisotropy is significantly large, as is the case in layered iron-selenides. To be quantitative and unambiguous about the shape of the OP, it is required to incorporate realistic FS topology, Fermi velocities, and density of states (DOS) at the Fermi level into the calculations.

To accomplish this goal, we focus on layered iron-selenide superconductors and study the information embedded in the angle-resolved specific heat coefficient, $\gamma = C/T$, and thermal conductivity, κ, in a rotating in-plane magnetic field using realistic tight-binding dispersions derived from first-principles electronic structure calculations. The main results of our calculations are: (1) For purely isotropic pairing symmetry, such as $s^{\pm}$, the moderate FS anisotropies of layered iron-selenide superconductors are sufficient to introduce field-angle dependent oscillations in the specific heat and thermal conductivity over a significant range of temperatures and at intermediate to high magnetic fields in the superconducting state. We find an inversion of the oscillation pattern as a function of temperature, which shows that the oscillations are not a simple consequence of the anisotropy of the upper critical field. Therefore not all such oscillations at intermediate fields can be taken as a proof of strong anisotropy in the superconducting gap. (2) For isotropic gap the oscillations in γ may change sign once or twice as a function of temperature. We identify the out-of-phase FS anisotropies between the bands as the source for two sign reversals. (3) Complex angle dependence of the specific heat and thermal conductivity on the field direction for anisotropic Fermi surfaces suggests that comparison of both quantities with material-specific theories is promising to identify the pairing symmetry and gap structure.

Formalism– In the iron selenides the Fe vacancy completely eliminates the hole pocket at the Γ point, and the FS consists of two concentric electron pockets at the M point, as follows from first-principles calculations [18] and photoemission spectroscopy [19]. Here, we use a first principles derived tight-binding parameterization of the electronic dispersion [9] with a weak k_z dispersion to obtain all necessary Fermi surface parameters. Cuts of the corresponding Fermi surfaces are shown in Fig. 1(a) with calculated normal-state DOS in 1(b) and moderately anisotropic Fermi velocities in 1(c).

We consider three nodeless gaps with s, $s^{\pm} = \cos k_x a + \cos k_y a$, and extended $\tilde{d}_{xy} = \sin(k_x a/2)\sin(k_y a/2)$ symmetry, shown in Fig. 1(d). Here $\tilde{d}$ means that the gap is

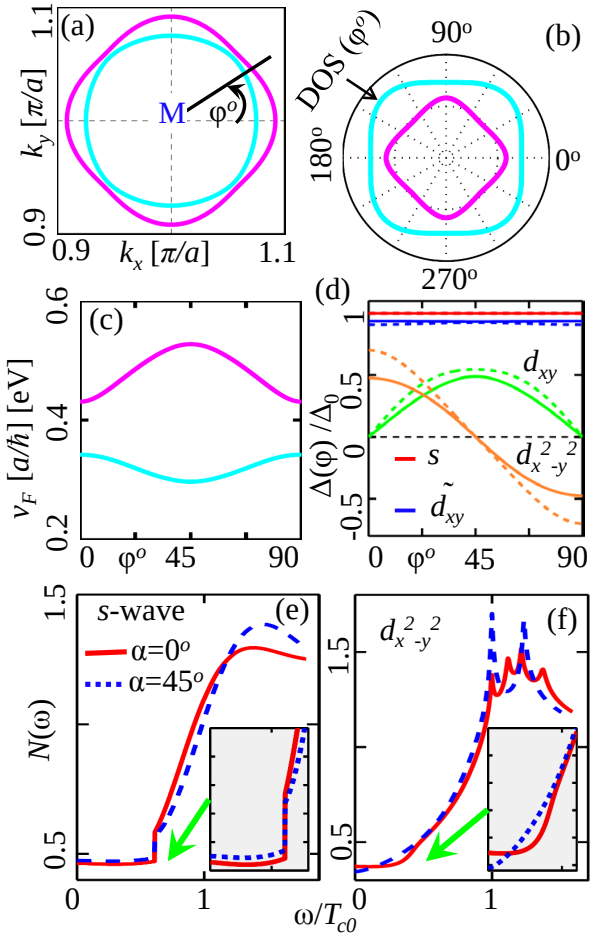

FIG. 1. (Color online) (a) Magenta and cyan colors show the electron-pocket Fermi surfaces (FSs) within the tight-binding model [9]. (b) Computed normal-state DOS at the Fermi level shown in polar plot for each band (same color as in (a)). (c) k_z-averaged in-plane Fermi velocities (lattice parameter $a = 4.2\,\text{Å}$) as a function of azimuthal FS angle ϕ. (d) Gap functions $\Delta_n(\phi)$ on FS1 (solid) and FS2 (dashed) for pairing symmetries considered. The nodeless states have negligible FS anisotropy. (e)-(f) Field-induced total DOS at $T = 0$ as a function of energy at two representative field angles $\alpha = \angle(\mathbf{H}, (100))$ for s and $d_{x^2-y^2}$ pairing; $H/H_{c2} = 0.5$ for s wave and 0.1 for $d_{x^2-y^2}$ wave.

extended and nodeless on the FS [9]. However, since all nodeless gaps exhibit very similar behavior, we will show detailed results only for isotropic pairing. Additionally, we consider two nodal gaps with $d_{x^2-y^2} = \cos k_x a - \cos k_y a$ and $d_{xy} = \sin k_x a \sin k_y a$ symmetry, with detailed results presented for $d_{x^2-y^2}$ pairing.

For magnetic field $\mathbf{H}$ applied at angle α with respect to the (100) direction, $\alpha = \angle(\mathbf{H}, (100))$, we compute the field-induced DOS within the extended Brandt-Pesch-Tewordt (BPT) quasiclassical approximation [20–22] by solving the transport equation for the multiband Green's function [17, 23–25]. We introduce band indices $n = 1, 2$ for the spatially averaged Green's function, g_n, and the angle-dependent DOS, $N_n(\omega, \hat{k}; \mathbf{H}) = -N_{fn}(\hat{k})\text{Im}\; g_n(\omega, \hat{k}; \mathbf{H})/\pi$, following the formulation of Ref. 24. The weight $N_{fn} = \int d\hat{k} N_{fn}(\hat{k})$ denotes the net normal-state DOS at the Fermi level in band n, where $\hat{k}$ is a point on the n-th FS, and $\int d\hat{k} \cdots \equiv \langle \ldots \rangle_{FS}$ is a compact notation for Fermi surface integrals. In our model the two bands are coupled only through the self-consistency equations for the superconducting OPs:

$$\Delta_n(\mathbf{H}, \hat{k}) = T \sum_{m,n'} \Big\langle V_{nn'}(\hat{k}, \hat{k}') N_{fn'}(\hat{k}') f_{n'}(\mathbf{H}, \hat{k}', \epsilon_m) \Big\rangle_{FS}. \tag{1}$$

Here f_n is the anomalous Gorkov function (off-diagonal Green's function) in the fermionic Matsubara notation. We assume that the pairing potential factorizes as $V_{nn'}(\hat{k}, \hat{k}') = V_{nn'} \mathcal{Y}_n(\phi) \mathcal{Y}_{n'}(\phi')$, with $\mathcal{Y}_n(\phi)$ the azimuthal angle-dependence of the superconducting gap, see Fig. 1, after projecting the OP of the appropriate symmetry on the Fermi surface of band n. For simplicity, we consider purely interband pairing $V_{12} = V_{21} = -V$ and eliminate V in favor of the transition temperature T_{c0} using weak-coupling theory [23].

The main approximation employed in the BPT approach is the averaging of the normal particle and hole propagators over the unit cell of the Abrikosov vortex lattice. This produces quantitatively correct results near the upper critical field for strongly type-II ($\kappa \gg 1$) superconductors, and, when complemented by the self-consistency of the OP, remains qualitatively valid over the range $0.5H_{c2} \lesssim H < H_{c2}$ [20, 26, 27]. For nodal or strongly anisotropic gaps the approach was argued to be valid down to low fields, where it yields results consistent with complementary treatments such as semiclassical method [17, 22, 28]. The self-consistent solution for the spatial dependence of the OP in the vortex lattice of anisotropic superconductors includes the admixture of higher order oscillator functions [17, 24, 25, 29, 30]. However, this admixture is small at least when the FS has rotational symmetry in the plane of field rotation [17], and for simplicity we neglect it.

The specific heat and thermal conductivity are calculated using the quasiclassical Green's function. To get a qualitative understanding of the field-angle results presented in this work, it is instructive to inspect the low-T approximations for $C = C_1 + C_2$ and $\kappa^{xx} = \kappa_1^{xx} + \kappa_2^{xx}$:

$$C_n(\alpha) \approx \int_{-\infty}^{\infty} d\omega \frac{\omega^2 \langle N_n(\omega, \hat{k}; \mathbf{H}) \rangle_{FS}}{4T^2 \cosh(\omega/2T)^2}, \tag{2}$$

$$\kappa_n^{xx}(\alpha) \approx \int_{-\infty}^{\infty} d\omega \frac{\omega^2 \langle v_n^x(\hat{k})^2 N_n(\omega, \hat{k}; \mathbf{H}) \tau_{n,\mathbf{H}}(\omega, \hat{k}) \rangle_{FS}}{2T^2 \cosh(\omega/2T)^2}, \tag{3}$$

where $\boldsymbol{v}_n$ is the Fermi velocity in each band and $\tau_{n,\text{H}}$ is the *transport* lifetime due to combined effects of impurity and vortex scattering [23]. In the normal state, $N_n(\omega, \hat{k}; \mathbf{H}) = N_{fn}(\hat{k}) \sim 1/|\boldsymbol{v}_n(\hat{k})|$ and $\tau_{n,\mathbf{H}} = \tau_{imp}$. Here, we consider the clean limit with purely intraband impurity scattering rate $1/\tau_{imp} = 0.01 \times 2\pi T_{c0}$ and the scattering phase shift $\delta = \pi/2$ (unitarity limit) with the pure transition temperature T_{c0}.

The anisotropy of the heat capacity at the lowest temperatures is determined by the residual DOS

$$N_n(\omega \approx 0, \mathbf{H}) \approx \left\langle N_{fn}(\hat{k}) \left[1 + \left(\frac{2\Lambda\Delta_n(\hat{k}, \mathbf{H})}{|\boldsymbol{v}_n^{\perp}(\hat{k})|} \right)^2 \right]^{-\frac{1}{2}} \right\rangle_{FS}, \tag{4}$$

where $\Lambda = (\hbar c/2|e|H)^{1/2}$ is the magnetic length, which is of order the coherence length ξ between $0.5H_{c2} < H < H_{c2}$, and $\boldsymbol{v}_n^{\perp}$ is the Fermi velocity perpendicular to the field $\mathbf{H}$ [23]. For nodal gaps and rotationally invariant single FS this yields an inversion of the oscillatory pattern at $T = 0$ and intermediate fields [17, 24, 31, 32]. Anisotropy of the Fermi surface introduces a more complex structure of $|\boldsymbol{v}_n^{\perp}(\hat{k})|$ and affects the profile of the DOS oscillations at zero energy [33–35], albeit the effect over the entire H-T phase diagram has not been explored. Multiband systems bring another complication since the relative contributions of each band to the net DOS depend not only on the amplitude and shape of the gap (in general $\Delta_1 \neq \Delta_2$), but also on the variations of the Fermi velocity with angle on each FS [36].

Results– Comparison with experimental results is facilitated by extracting the harmonics of the full angle-dependent profile of $\gamma(\alpha)$ and $\kappa(\alpha)$ and comparing with the expected gap variation [15, 23, 25, 37]. For Fermi surfaces with cylindrical symmetry only twofold and fourfold harmonics are significant [15, 25], while for multiple FS and anisotropic band dispersions the profiles of γ and κ are more complex [23]. We estimate the amplitudes of the fourfold thermal oscillations as $C_{4\alpha} = \Pi_0^C - \Pi_{45}^C$, where $\Pi_\alpha^C = \gamma(\alpha;T)/\gamma(T_c)$ and $\kappa_{4\alpha} = [\Pi_0^\kappa + \Pi_{90}^\kappa]/2 - \Pi_{45}^\kappa$, where $\Pi_\alpha^\kappa = [\kappa^{xx}(\alpha;T)T_c]/[\kappa^{xx}(T_c)T]$. The definition of $\kappa_{4\alpha}$ corrects for the (usually large) twofold anisotropy between the heat current flowing parallel vs. perpendicular to the vortex lines. In Fig. 2, we show $\gamma(\alpha)$ and $\kappa(\alpha)/T$ at representative low fields for an isotropic gap ($H/H_{c2} = 0.5$) and a nodal $d_{x^2-y^2}$ gap ($H/H_{c2} = 0.1$). The amplitudes of the corresponding fourfold terms are plotted in the lower panels.

The features for the d-wave model qualitatively reproduce the results of calculations with quasi-two-dimensional model Fermi surfaces: there are two inversions of the anisotropy, one at high temperatures close to the transition to the normal state, and the other at low T, characteristic of the change from energy-shift dominated to vortex-scattering dominated regimes [17, 23]. Figs. 2(c2) and (d2) clearly show the inversion at low temperatures and fields, while the high-T inversion is identifiable in γ, but not easily seen in κ/T. The exact locations of the inversion lines in the H-T phase diagram depend on the specific definitions for extracting the fourfold term, however, their existence is a robust feature.

The situation here is much more complex than for a FS with cylindrical symmetry, since the interplay of the d-wave symmetry in Δ_n and higher order functions in $v_n^{\perp}$ give rise to rather intricate behavior as a function of the angle. This becomes evident from our results for a nodeless isotropic gap, Figs. 2(a1) and (b1), where the features due to the Fermi surface anisotropy control the oscillations (note the difference in the overall scale). At $H/H_{c2} = 0.5$ the BPT approach at best works only qualitatively, however, the results are characteristic of all higher T and H, where the method is quantitatively accurate; this is also clear from the continuity of the inversion lines in the phase diagram of Fig. 3. The thermal conductivity shows several features attributable to the Fermi surface anisotropy, and, notably, there is a sign reversal of the fourfold term at high T. At low T no inversion is visible in $\kappa_{4\alpha}$, but the overall shape of the variation of $\kappa(\alpha)$ in Fig. 2(a1) clearly does not allow for fit by only two harmonics, hence this conclusion is sensitive to the exact definition of $\kappa_{4\alpha}$.

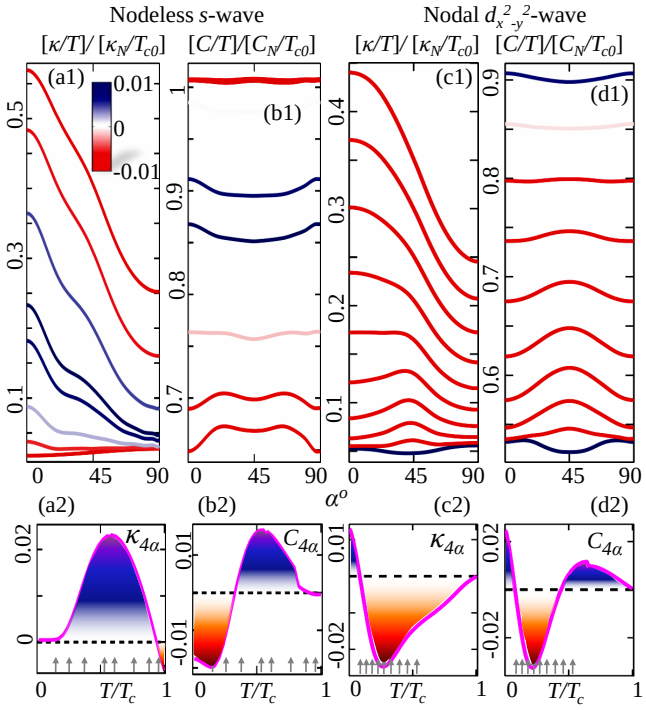

FIG. 2. (Color online) (a1) Thermal conductivity κ/T along (100) direction (normalized to its normal-state value κ_N/T_c) as a function of in-plane field angle α at fixed $H/H_{c2} = 0.5$ for s wave, plotted from low to high temperatures (bottom to top curves). All curves are shifted vertically by 0.01 for clarity. Each curve is colored by the amplitude of the fourfold oscillation given in (a2); a uniform color map is used for values below -0.01 and above 0.01. (a2) The fourfold amplitude of κ/T is plotted as a function of T. The vertical arrows in the bottom row depict the temperatures at which curves in the top panel are shown. Panels (b1)-(b2): Specific heat for same parameters as in (a1)-(a2). Panels (a) and (b) are for purely isotropic s-wave case, while similar plots in (c) and (d) are shown for nodal $d_{x^2-y^2}$ symmetry at $H/H_{c2} = 0.1$.

The calculations show a very weak (or no) sign change in $C_{4\alpha}$ at high temperatures and a prominent inversion at low T ($T \approx T_c/4$). The inversion of the anisotropy for isotropic gap at intermediate fields is the key feature found here. If the oscillations in κ and γ were a simple manifestation of the low-temperature anisotropy of the upper critical field in the rotation plane, the inversion would not occur. Its pres-

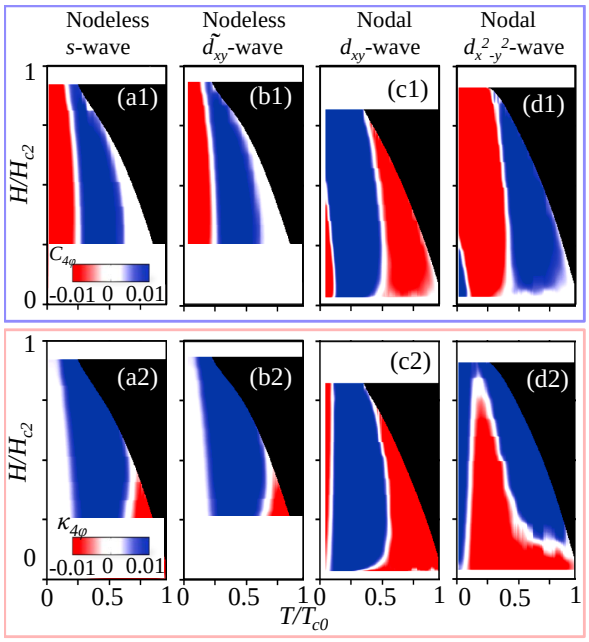

FIG. 3. (Color online) Contour plots of fourfold amplitude oscillations of specific heat, $C_{4\alpha}$ (top row), and thermal conductivity $\kappa_{4\alpha}$ (bottom row) in the H-T phase diagram. Each column denotes a different gap symmetry. All plots use the same color map (red to blue); a uniform color map is used for values below -0.01 and above 0.01. Note the fourfold amplitude is given with respect to $H//(100)$, i.e., a negative value corresponds to a minimum at $\alpha = 0^o$. T_c(H) is defined by the vanishing of both OPs for each gap symmetry, which determines the line of the upper critical field $H_{c2}(T;\alpha)$.

ence shows the crucial role of the Fermi surface shape and the anisotropy in the quasiparticle band dispersion. We also note that the similarity between the loci of the inversion lines in the T-H plane for $C_{4\alpha}$ and $\kappa_{4\alpha}$ found for the nodal gaps on the rotationally symmetric Fermi surfaces [25] does not appear here. The difference is presumably due to different weights of particular regions in the Fermi surface averages for the specific heat ($\propto N_{fn}(\hat{k})$) and the thermal conductivity ($\propto v_n^x(\hat{k})^2 N_{fn}(\hat{k})|$). For nodal or strongly anisotropic gaps these averages are strongly weighted towards the regions of smallest $\Delta_n(\hat{k})$, an effect absent for isotropic pairing.

In Fig. 3, we show the contour plot of the amplitude of the fourfold oscillation extracted from γ (top row) and κ/T (bottom row) for two nodeless and two nodal gaps. For a rotationally invariant Fermi surfaces the specific heat oscillation simply changes sign between the d_{xy} and $d_{x^2-y^2}$ symmetries [24]. Difference in the location of the inversion lines in Fig. 3(c1) and (d1) is therefore attributable to the FS anisotropy. The intriguing result here is both low-T and high-T sign reversals in γ for a fully isotropic gap, see Fig. 3(a),(b). We verified that the high-T inversion remains at nearly the same location in a single-band superconductor with an identical Fermi surface, but the low-T feature does not appear in that case. Nor do we find this sign change for two-band models with similar (in-phase) angular variations of the quasiparticle velocity along each of the Fermi surfaces. The only situation where we obtain this additional inversion is when the amplitudes of the FS velocities on the respective FSs are "out of phase": along a particular azimuthal direction, ϕ, the Fermi velocity $v_1(\phi)$ is large (compared to the FS average), while $v_2(\phi)$ is small.

We note that our discussion of the anisotropy for systems with isotropic gaps is restricted to moderate-to-high fields. At low fields the BPT approximation breaks down, and we expect very small electronic contributions to both specific heat and the thermal conductivity. Therefore a significant anisotropy observed in the single-layer $FeSe_{0.45}Te_{0.55}$ at fields below 10% of H_{c2} [38] is consistent with the deep minima or nodes in the gap.

Conclusions– We studied oscillations in the specific heat and thermal conductivity with respect to a rotating in-plane magnetic field for various gap symmetries in a multiband superconductor. We used realistic tight-binding dispersions derived from electronic structure calculations for the newly discovered $A_yFe_2Se_2$ superconductors, where the pairing symmetry is still debated. Our detailed calculations show two sign reversals at intermediate fields in the oscillations of the field-angle resolved specific heat versus temperature, irrespective of the gap symmetry and anisotropy, whereas the thermal conductivity shows a more complex dependence on the gap structure. Consequently, realistic model calculations together with combined measurements of oscillations in both the specific heat and thermal conductivity under rotated field and complemented by measurements of the power-law temperature dependence at zero field can help identify the gap anisotropy. Finally, our calculations predict the observation of fourfold oscillations and sign reversals for Fe_2Se_2-based compounds.

We thank R. Movshovich and A. V. Balatsky for discussions and encouraging this study. This work is funded in part by the US DOE under Grants No. DE-AC52-06NA25396 (T.D. and M. J. G.) and DE-FG02-08ER46492 (I. V.), by NSF Grant No. DMR 0954342 (A. B. V.), and by the Office of Science (BES) through a NERSC computing allocation of the U.S. DOE under contract No. DE-AC02-05CH11231.

[1] I. I. Mazin *et al.*, Phys. Rev. Lett. **101**, 057003 (2008).
[2] K. Kuroki *et al.*, Phys. Rev. B **79**, 224511 (2009).
[3] A.V. Chubukov *et al.* Phys. Rev. B **78**, 134512 (2008).
[4] Y. Bang and H.-Y. Choi, Phys. Rev. B **78**, 134523 (2008).
[5] J. Guo *et al.*, Phys. Rev. B **82**, 180520(R) (2010); A. Krzton-Maziopa, *et al.*, J. Phys.: Condens. Matter **23** 052203 (2011); M. Fang, *et al.*, Europhys. Lett. **94** 27009 (2011).
[6] I. I. Mazin *et al.* Phys. Rev. B **84**, 024529 (2011).
[7] R. Yu *et al.* arXiv:1103.3259.
[8] T. Saito *et al.*, Phys. Rev. B **83**, 140512(R) (2011).
[9] T. Das and A. V. Balatsky, Phys. Rev. B **84**, 014521 (2011); Phys. Rev. B **84**, 115117 (2011).
[10] T. A. Maier *et al.*, Phys. Rev. B **83**, 100515 (2011)
[11] F. Wang *et al.* Europhys. Lett. **93**, 57003 (2011).
[12] Z. Shermadini, *et al.* Phys. Rev. Lett. **106**, (2011) 117602

[13] H. Kotegawa, Y. Hara, H. Nohara, H. Tou, Y. Mizuguchi, H. Takeya, and Y. Takano, J. Phys. Soc. Jpn. **80**, (2011) 043708.
[14] D. A. Torchetti, *et al.* Phys. Rev. B **83**, (2011) 104508.
[15] Y. Matsuda *et al.* J. Phys.: Condens. Matter **18**, R705 (2006).
[16] P. Miranovic *et al.* J. Phys.: Condens Matter **17**, 7917 (2005).
[17] A. B. Vorontsov and I. Vekhter, Phys. Rev. Lett **96**, 237001 (2006).
[18] Y. Zhang *et al.* Nature Materials **10**, 273 (2011)
[19] X.-P. Wang *et al.* Europhys. Lett. **93**, 57001 (2011);
[20] U. Brandt, W. Pesch, and L. Tewordt, Z. Phys. **201**, 209 (1967).
[21] W. Pesch, Z. Phys. B **21**, 263 (1975).
[22] A. Houghton and I. Vekhter, Phys. Rev. B **57**, 10831 (1998).
[23] A. B. Vorontsov and I. Vekhter, Phys. Rev. Lett **105**, 187004 (2010).
[24] A. B. Vorontsov and I. Vekhter, Phys. Rev. B **75**, 224501 (2007).
[25] A. B. Vorontsov and I. Vekhter, Phys. Rev. B **75**, 224502 (2007).
[26] E. H. Brandt, J. Low Temp. Phys. **24**, 409 (1976).
[27] J. M. Delrieu, J. Low Temp. Phys. **6**, 197 (1972).
[28] T. Dahm *et al.*, Phys. Rev. B **66**, 144515 (2002).
[29] I. A. Lukyanchuk and V. P. Mineev, Zh. Eksp. Teor. Fiz. **93**, 2045 (1987) [Sov. Phys. JETP **66**, 1168 (1987)].
[30] H. Won and K. Maki, Phys. Rev. B **53**, 5927 (1996).
[31] M. Udagawa, Y. Yanase, and M. Ogata, Phys. Rev. B **70**, 184515 (2004).
[32] P. Miranoviċ, N. Nakai, M. Ichioka, and K. Machida, Phys. Rev. B **68**, 052501 (2003).
[33] M. Udagawa, Y. Yanase, and M. Ogata, Phys. Rev. B **71**, 024511 (2005).
[34] Y. Nagai *et al.*, J. Phys.: Conf. Ser. **150**, 052177 (2009)
[35] Y. Nagai *et al.*, Phys. Rev. B **76**, 214514 (2007).
[36] Y. Nagai, H. Nakamura, M. Machida, Phys. Rev. B **83**, 104523 (2011).
[37] M. Yamashita, *et al.*, Phys. Rev. B **84**, 060507(R) (2011)
[38] B. Zheng *et al*, Nat. Comms. **1**, 112 (2010); doi: 10.1038/ncomms1115